SLAC-PUB-12827
Revised-October 2007

The Astrophysical Journal, accepted 2007 October 8
Preprint typeset using LaTeX style emulateapj v. 04/21/05

# PARAMETERIZATION OF THE ANGULAR DISTRIBUTION OF GAMMA RAYS PRODUCED BY P-P INTERACTION IN ASTRONOMICAL ENVIRONMENT

Niklas Karlsson[1] and Tuneyoshi Kamae[2,3]
Stanford Linear Acceleration Center, Menlo Park, CA 94025
*Submitted 2007 August 17; accepted 2007 October 8*

## ABSTRACT

We present the angular distribution of gamma rays produced by proton-proton interactions in parameterized formulae to facilitate calculations in astrophysical environments. The parameterization is derived from Monte Carlo simulations of the up-to-date proton-proton interaction model by Kamae et al. (2005) and its extension by Kamae et al. (2006). This model includes the logarithmically rising inelastic cross section, the diffraction dissociation process and Feynman scaling violation. The extension adds two baryon resonance contributions: one representing the $\Delta(1232)$ and the other representing multiple resonances around 1600 MeV/$c^2$. We demonstrate the use of the formulae by calculating the predicted gamma-ray spectrum for two different cases: the first is a pencil beam of protons following a power law and the second is a fanned proton jet with a Gaussian intensity profile impinging on the surrounding material. In both cases we find that the predicted gamma-ray spectrum to be dependent on the viewing angle.

*Subject headings:* cosmic rays — galaxies: jets — gamma rays: theory — ISM: general — neutrinos — supernovae: general

## 1. INTRODUCTION

Gamma-ray emission due to decays of neutral pions produced in proton-proton (p-p) interactions has been predicted from the Galactic ridge, supernova remnants (SNRs), active galactic nucleus (AGN) jets, and other astronomical sites (Hayakawa 1969; Stecker 1970; Murthy & Wolfendale 1986; Schönfelder 2001; Schlickeiser 2002; Aharonian 2004). A multitude of gamma-ray sources are already known today (see, e.g., Hartman et al. 1999) and with new gamma-ray observatories covering GeV to TeV energies many more are expected to be found (Aharonian et al. 2003, 2004a,b, 2005; Ong 1998; Schroedter et al. 2005; Schönfelder 2001; Weekes 2003). The GeV energy window, in particular above about 10 GeV, has been poorly explored and the GLAST Large Area Telescope (GLAST-LAT)[4] is expected to provide high-statistics data in this window.

Interpretation of the observed gamma-ray spectra and identification of the involved interactions require not only high-quality observational data, but also good knowledge of the contributing production mechanisms. In the high-energy regime (sub-GeV to multi-TeV energies), the two dominant processes for gamma-ray production are p-p interactions and subsequent decays of neutral pions and inverse Compton (IC) up-scattering of low-energy photons on high-energy electrons. Production of gamma rays through pion decay relies on acceleration of cosmic ray primaries, protons or heavier nuclei, to high energies.

The diffuse gamma-ray emission from the Galactic ridge was first detected by the OSO-3 and SAS-2 satellites and later the COS-B and EGRET instruments. This emission is interpreted as predominantly due to decays of neutral pions produced in interactions between accelerated protons or heavier nuclei with the interstellar medium (ISM; Stecker 1973, 1989; Strong et al. 1978, 1982, 2000, 2004, 2007; Stephens & Badhwar 1981; Dermer 1986a; Hunter et al. 1997). The gamma-ray flux and spectral shape measured by EGRET (Hunter et al. 1997) is considered as the key attestation of this interpretation. There is also significant contribution to the diffuse gamma-ray emission from IC scatterings, in particular in the Galactic ridge (Murthy & Wolfendale 1986; Strong et al. 2000; Schönfelder 2001).

Several SNRs have been detected in TeV energies with ground based Air Cherenkov Telescopes (ACTs), including the shell-type SNRs RX J1713.7-3946 and RX J0852.0-4622 (Aharonian et al. 2004a, 2005). Observations in the X-ray band from both RX J1713.7-3946 (Koyama et al. 1997; Slane et al. 1999; Uchiyama et al. 2003) and RX J0852.0-4622 (Tsunemi et al. 2000; Iyudin et al. 2005) show a smooth, featureless spectrum indicating synchrotron X-ray emission due to a population of TeV electrons. The same electron population might also produce high-energy gamma rays through IC scatterings, but the measured gamma-ray fluxes and spectra in TeV energies do not fully match the predicted ones (see, e.g., the analysis in Uchiyama et al. 2003), and it has been suggested that there might also be a significant component due to hadronic interactions with the surrounding ISM (Berezhko & Volk 2000; Enomoto et al. 2002; Aharonian 2004; Katagiri et al. 2005). Hadronic models fit the very-high-energy gamma-ray spectrum assuming a beam of accelerated protons (Moskalenko et al. 2007). The highest-energy cosmic rays (CRs) escape the forward shock region of the SNR almost unidirectionally; the gamma-ray spectrum becomes angular dependent.

High-energy gamma-ray emission from AGN jets is usually explained using leptonic models with electrons accelerated to TeV energies. Support for this comes from

Electronic address: niklas@slac.stanford.edu
[1] Visiting scientist from the Royal Institute of Technology, AlbaNova University Center, SE-106 91 Stockholm, Sweden
[2] Also with the Kavli Institute for Particle Astrophysics and Cosmology, Stanford University, Menlo Park, CA 94025
[3] Electronic address: kamae@slac.stanford.edu
[4] GLAST Large Area Telescope, http://www-glast.stanford.edu.

the observed radio and X-ray spectra which match those of synchrotron radiation from high-energy electron populations. The apparent synchronization in the observed variability of X-ray and gamma-ray fluxes gives further support for the leptonic modeling (Ong 1998; Schönfelder 2001; Schlickeiser 2002; Aharonian 2004). There are observations of AGN jets where the leptonic scenario faces difficulties. For these jets gamma-ray production through p-p interactions has been put forward as an alternative (Mücke & Protheroe 2001; Mücke et al. 2003; Böttcher & Reimer 2004).

The giant radio galaxy M87 has recently been observed in TeV energies with the H.E.S.S. Cherenkov telescopes (Beilicke et al. 2005). The jet is aligned about 30° (Bicknell & Begelman 1996) relative to the line of sight and it has been well studied in radio, optical and X-ray wavelengths. The central object is supposedly a supermassive black hole. Stawarz et al. (2006) interpret the TeV emission as due to Componization of synchrotron radiation from a flare in the nucleus. Reimer et al. (2004), on the other hand, have suggested the Synchrotron-Proton Blazar (SPB) model as the production mechanism for the TeV gamma-ray emission. The SPB model require protons to be accelerated to extremely high energies making it less favorable. Another possibility is accelerated protons leaking out of the jet near the central object, interacting with surrounding material and producing gamma-rays through the decay of neutral pions.

In this paper the angular distribution of gamma rays produced in proton-proton interactions is presented in parameterized formulae. These are derived from Monte Carlo simulations of the up-to-date proton-proton interaction model by Kamae et al. (2006). The angular distribution is given relative to the incident proton direction. With this formalism, the gamma-ray spectrum can be calculated for any given distribution of protons, including angular dependent ones.

Parameterization of the angular distributions of other stable secondary particles, i.e. electrons, positrons and neutrinos, has been deferred due to observational limitations. When high statistics neutrino data becomes available (Halzen 2005) it may be worth while extending the parameterization to include the angular distribution of neutrinos.

It is noted that Koers et al. (2006) have taken another approach and parameterized the energy and rapidity distributions of pions and kaons and from this they are able to derive the spectrum and angular distribution of gamma rays. They consider proton energies above 1 TeV and therefore their model is not suited for studies in the GLAST-LAT energy range. In this paper, proton energies from the pion production threshold and the resonance region up to about $10^5$ GeV are considered. High-precision data is expected from the GLAST-LAT in the GeV range which makes it important with a parameterization covering this range.

## 2. PROTON-PROTON INTERACTION MODEL

For this work the proton-proton interaction model used to calculate the diffuse Galactic gamma-ray flux (Kamae et al. 2005) and its extension (Kamae et al. 2006) is adopted. In an effort to predict the contribution to the Galactic diffuse emission from $\pi^0$ decays, Kamae et al. (2005) found that past calculations (Stecker 1970, 1973, 1989; Strong et al. 1978; Stephens & Badhwar 1981; Dermer 1986a,b; Mori 1997) left out two important features of the inelastic p-p interaction, the diffraction dissociation process and the Feynman scaling violation. It was also noted that past calculations assumed an energy independent inelastic p-p cross section, about 24 mb for $T_p \gg 10$ GeV, in contradiction to recent experimental data where a logarithmic increase of the cross section with the incident proton energy is evident (Hagiwara et al. 2002). The predicted gamma-ray spectrum changed significantly in the GeV energy range when the above features were included. The power-law index of the gamma-ray spectrum is about 0.05 lower in absolute value than that of the incident proton spectrum and the gamma-ray flux is increased significantly compared to the reference scaling model (Kamae et al. 2005); the increase is proton energy dependent, about 10-20% in the low-GeV range and about 50% above a few 100 GeV. From here on, the model by Kamae et al. (2005) is referred to as model A.

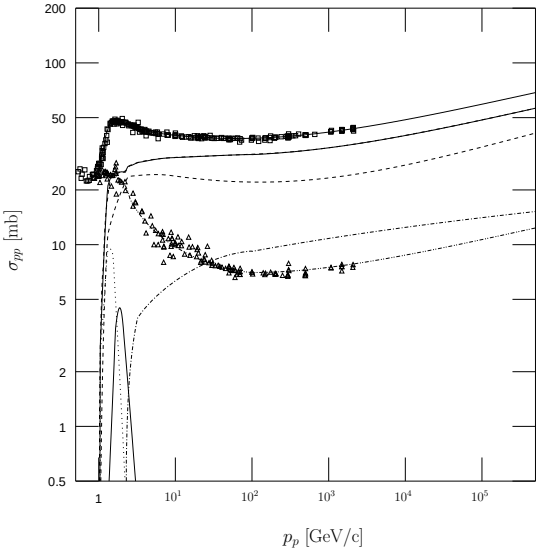


FIG. 1.— Experimental $p-p$ cross sections, as a function of proton momentum, and that of adjusted model A: experimental total (squares), experimental elastic (triangles), total inelastic (thick solid line), non-diffractive (dashed line), diffractive process (dot-dashed line), $\Delta(1232)$ (dotted line), and res(1600) (thin solid line). The total inelastic is the sum of the four components. The thin solid and dot-dot-dashed lines running through the two experimental data sets are eye-ball fits to the total and elastic cross sections, respectively. The functional forms are those given by equations (1) through (4) in Kamae et al. (2006).

Model A was primarily aimed at studying the diffuse emission from the Galactic ridge and thus concerned proton kinetic energies well above 1 GeV. It is not accurate near the pion production threshold (see Figure 5 of Kamae et al. 2005). To correct for this and improve the accuracy for lower proton momenta, Kamae et al. (2006) adjusted model A by including contributions from two baryon resonance excitation states, $\Delta(1232)$, representing the physical $\Delta$ resonance with a mass of 1232 MeV/$c^2$, and res(1600), representing several resonances with masses around 1600 MeV/$c^2$. The term "baryon resonance" refers to both nucleon resonances with iso-spin 1/2 and $\Delta$ resonances with iso-spin 3/2. The $\Delta(1232)$ decays to a nucleon (proton or neutron) and one pion ($\pi^+$, $\pi^0$ or $\pi^-$; Hagiwara et al. 2002) and

the other resonance, res(1600), is assumed to decay to a nucleon and two pions. The extension of model A which includes the baryon resonances is from here on referred to as adjusted model A.

Other necessary adjustments to model A forced by the introduction of the baryon resonance contributions is described in Kamae et al. (2006, section 3). This includes the adjustment of the non-diffractive inelastic p-p cross section to accommodate for the resonances while not exceeding the total inelastic cross section. The total inelastic p-p cross section is shown in Figure 1 together with the four component cross sections of adjusted model A.

Due to paucity of experimental data, $\alpha-p$, $p$-He and $\alpha$-He have not been included in this work. Near the Earth about 7% of the CR flux is $\alpha$-particles (Schlickeiser 2002) and the ISM contains about 10% He by number. Both the $\alpha$-particle and the He nucleus can be approximated as four individual nucleons. The error from such an approximation is expected to be less than 10% for high-energy gamma rays. Fermi motion of nucleons and multiple nucleonic interactions in the nucleus affect the pion production near the threshold and in the resonance region ($T_p < 3$ GeV; Crawford et al. 1980; Mårtensson et al. 2000). This will enhance the pion multiplicity below 100 MeV. The need for separate treatment of interactions such as p-He, $\alpha$-p, and $\alpha$-He is acknowledged.

## 3. MONTE CARLO SIMULATIONS

The parameterization of the angular distribution of gamma rays is derived from Monte Carlo simulations on the adjusted proton-proton interaction model A as given in Kamae et al. (2006). Events were generated for each of the four components, the non-diffractive interaction, the diffraction dissociation process and the two resonance excitation processes in the following way. For the non-diffractive interaction in the high energy range ($T_p > 52.6$ GeV) Pythia 6.2 (Sjöstrand et al. 2001) was used with the option for multi-parton scaling violation (Sjöstrand & Skands 2004).[5] This was complemented with the parameterization of inclusive pion cross sections by Blattnig et al. (2000) in the low energy range ($T_p < 52.6$ GeV). The diffraction dissociation process was simulated with a Monte Carlo code by T. Kamae (2004, personal communications)[6] and the resonance excitation components were simulated with Monte Carlo codes by T. Kamae (2005, personal communications).

For each of the four components mentioned above, events were generated for discrete proton kinetic energies (0.488 GeV $\leq T_p \leq$ 512 TeV) taken from a geometrical series

$$T_p = 1000 \cdot 2^{(i-22)/2} \text{ GeV}, \; i = 0, \ldots, 40. \qquad (1)$$

Each proton kinetic energy, $T_p$, represents a bin covering $2^{-0.25}T_p$ to $2^{0.25}T_p$. The addition of the resonances to the model required an increased sampling frequency near the pion production threshold and events were also generated for $T_p = 0.58$ GeV and 0.82 GeV. Events were not generated for proton energies where the component cross section is very small or zero.

[5] See http://cepa.fnal.gov/CPD/MCTuning1 and http://www.phys.ufl.edu/∼rfield/cdf

[6] It is acknowledged that the latest version of Pythia includes the diffractive interaction and that the code used here agrees with Pythia. The Monte Carlo code is available upon request.

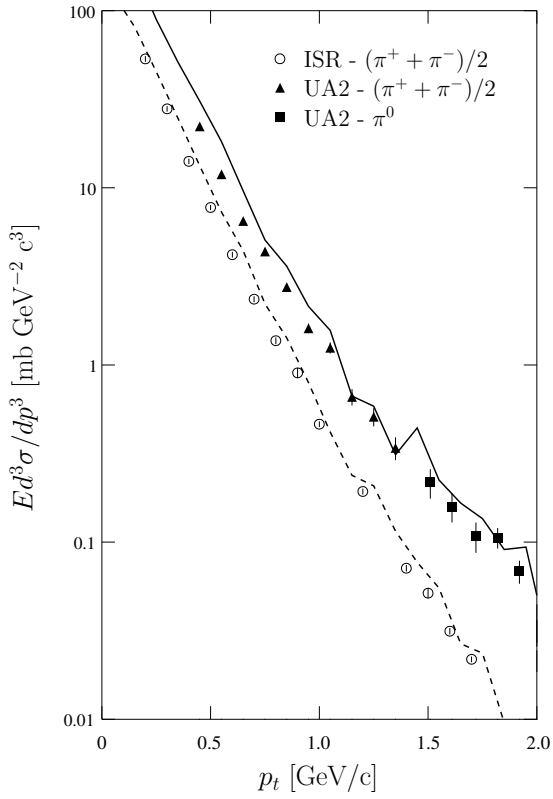


FIG. 2.— Experimental invariant cross section $Ed^3\sigma/dp^3$ at production angle $\theta_{\rm cms} = 90°$ and beam energy $\sqrt{s} = 540$ GeV for $(\pi^+ + \pi^-)/2$ (filled triangles) and $\pi^0$ (filled squares) measured by the UA2 collaboration ($\bar{p}p$ collider experiment; Banner et al. 1982, 1983) and beam energy $\sqrt{s} = 53$ GeV for $(\pi^+ + \pi^-)/2$ (open circles) measured at the ISR ($pp$ collider; Alper et al. 1975) together with the $\pi^0$ invariant cross section calculated from Monte Carlo simulations in this work at $T_p = 181$ TeV ($\sqrt{s} = 582$ GeV, solid line) and $T_p = 1.41$ TeV ($\sqrt{s} = 51.5$ GeV, dashed line).

### 3.1. *Pion Transverse Momentum*

The above described Monte Carlo simulations have been verified to agree with experimental data available for pions. The inclusive $\pi^0$ cross section was verified to agree with the experimental one and the simulations were ensured to reproduce the distributions of pion kinetic energy in the p-p center-of-mass (CM) system in the resonance region (Kamae et al. 2006).

For this work, the $\pi^0$ transverse momentum distribution was compared with those measured with accelerator experiments. Figure 2 shows the invariant $\pi^0$ cross section, $Ed^3\sigma/dp^3$, at production angle $\theta_{\rm cms} = 90°$ for proton kinetic energies $T_p = 1.41$ TeV ($\sqrt{s} = 51.5$ GeV) and 181 TeV ($\sqrt{s} = 582$ GeV) together with experimental data for $\pi^\pm$ measured at the ISR at $\sqrt{s} = 53$ GeV (Alper et al. 1975) and by the UA2 collaboration at $\sqrt{s} = 540$ GeV (Banner et al. 1982, 1983). One must note that the ISR was a $pp$ collider and that UA2 was a $\bar{p}p$ collider experiment. The distributions follow the expected exponential form for small $p_t$.

In addition, the energy dependence of the average transverse momentum, $\langle p_t \rangle$, calculated from Monte Carlo event data was compared with that from ISR experiments. In accelerator experiments it is difficult to measure $\pi^0$ directly but one can expect that $\langle p_t[\pi^0] \rangle \simeq \langle p_t[\pi^\pm] \rangle$ (Alner et al. 1987). $\langle p_t[\pi^0] \rangle$ was calculated with-

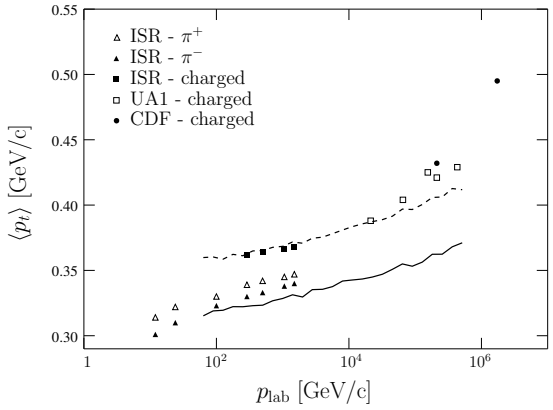


FIG. 3.— Average transverse momentum, $\langle p_t \rangle$, for production of pions and all charged particles ($\pi^{\pm}$, $K^{\pm}$ and protons) versus the laboratory momentum. Data points are for $\pi^+$ (open triangles), $\pi^-$ (filled triangles) and all charged particles (filled squares) from ISR, all charged particles (filled diamonds) from UA1 and all charged particles (filled circles) from CDF. ISR data are from $pp$ collider experiments and are taken from Rossi et al. (1975) and UA1 and CDF data are from $\bar{p}p$ collider experiments and are taken from Abe et al. (1988). Lines are for $\pi^0$ (solid line) and all charged particles (dashed line) from Monte Carlo simulations in this work.

out any fitting and Figure 3 shows the average transverse momentum as a function of the proton momentum in the laboratory frame. Rossi et al. (1975) estimated the error on $\langle p_t[\pi^{\pm}] \rangle$ to be about 10% and $\langle p_t[\pi^0] \rangle$ calculated here is within this error margin.

At very high proton momentum experimental data is in general limited to the average transverse momentum of charged particles, $\langle p_t[\text{charged}] \rangle$, where charged particles include charged pions and kaons and protons. Again, without fitting, $\langle p_t[\text{charged}] \rangle$ was calculated from Monte Carlo event data and compared with experimental data measured at the ISR and by the UA1 and CDF collaborations.[7] As can been seen in Figure 3 the difference is on the order of a few percent except at very high energies. The discrepancy in average transverse momentum at high proton momentum is inherent to Pythia 6.2 which has not been fine-tuned to the highest energy data available from CDF (T. Sjöstrand 2007, personal communications).

### 3.2. *Angular Distribution of Gamma Rays*

The Monte Carlo simulations generate data on momentum, $\mathbf{p} = (p_x, p_y, p_z)$, and total energy, $E$, for each gamma-ray photon. Since the incident proton direction in the simulations is along the z-axis the transverse momentum, $p_t$, is simply

$$p_t = \sqrt{p_x^2 + p_y^2} \tag{2}$$

and this was calculated for each simulated event. Events were then binned in 2D histograms,

$$\frac{\Delta^2 N}{\Delta \log(E) \Delta p_t}, \tag{3}$$

over total energy, $E$, and transverse momentum, $p_t$, with one histogram per proton kinetic energy. Bins widths were taken to be $\Delta \log(E) = 0.05$ and $\Delta p_t = 10$ MeV/c.

[7] Note again that ISR was a $pp$ collider and that UA1 and CDF are $\bar{p}p$ collider experiments.

Normalization to the proton-proton inelastic cross section, $\sigma_{pp}$ (given by eqs. (1) through (4) in Kamae et al. 2006), and per proton-proton interaction gives the differential cross section

$$\frac{\Delta^2 \sigma}{\Delta \log(E) \Delta p_t} = \frac{\sigma_{pp}}{N_{pp}} \frac{\Delta^2 N}{\Delta \log(E) \Delta p_t}, \tag{4}$$

where $N_{pp}$ is the number of proton-proton events simulated and $\Delta N$ is the number of gamma rays in a given bin. This differential cross section is a representation of the angular distribution of gamma rays.

## 4. PARAMETERIZATION OF GAMMA-RAY TRANSVERSE MOMENTUM DISTRIBUTIONS

For each proton kinetic energy, $T_p$, the transverse momentum distribution is parameterized as

$$\frac{\Delta^2 \sigma}{\Delta \log(E) \Delta p_t} = p_t F(p_t, x) F_{\rm kl}(p_t, x), \tag{5}$$

where $x = \log(E[\text{GeV}])$, $F(p_t, x)$ is the function representing the differential cross section $\Delta\sigma/\Delta p_t^2$ and $F_{\rm kl}(p_t, x)$ is used to approximately enforce the energy-momentum conservation. Assuming axial symmetry around the $p_{\parallel}$ axis, phase space is proportional to $dp_t^2 dp_{\parallel} = 2 p_t dp_t dp_{\parallel}$, which gives the extra factor of $p_t$ in equation (5).

The function $F_{\rm kl}(p_t, x)$ enforcing the energy-momentum conservation is taken to be

$$F_{\rm kl}(p_t, x) = \frac{1}{\exp\left(W(p_t - L_p)\right) + 1}, \tag{6}$$

where $W = 75$ and

$$L_p = \begin{cases} 0.0976 + 0.670 \exp(1.81x) & x < -1 \\ -0.793 + \exp(0.271(x+1)) & \\ \quad +0.363(x+1)^2) & -1 \le x < 0.5 \\ 2.5 & x \ge 0.5, \end{cases} \tag{7}$$

with $x = \log(E[\text{GeV}])$.

In contrast to the parameterization of inclusive cross sections by Kamae et al. (2006), where the non-diffractive and the diffraction contribution were treated separately, the two are here merged to one contributing component. This is well justified in astrophysical contexts. The new component is from here on referred to as the non-resonance component.

The $p_t$ distribution is given by 2D histograms, one histogram per proton kinetic energy, $T_p$, and component: non-resonance, $\Delta(1232)$, and res(1600). Each histogram is fitted in slices along $p_t$, i.e. each slice $\Delta\sigma/\Delta p_t^2$ covers one bin of $\Delta \log(E)$. Note that $\Delta\sigma/\Delta p_t^2$ does not imply integrating over $\log(E)$.

For the non-resonance component $\Delta\sigma/\Delta p_t^2$ is expected to follow an exponential form

$$F_{\rm nr}(p_t, x) = a_0 \exp\left(-\frac{p_t}{a_1}\right). \tag{8}$$

Parameter $a_1$ gives the shape of the differential cross section and $a_0$ gives the absolute normalization. When integrating over $p_t$ one should recover the inclusive cross section $\Delta\sigma/\Delta \log(E)$, i.e.

$$\int_0^{\infty} \frac{\Delta\sigma}{\Delta p_t^2} dp_t = \frac{\Delta\sigma}{\Delta \log(E)}. \tag{9}$$

TABLE 1
Parameters describing transverse momentum distributions

| Parameters | Formulae as functions of the proton kinetic energy, $y = \log(T_p[\mathrm{TeV}])$ |
|---|---|
| | Non-resonance, eq. (12) |
| $a_{10}$ ..... | $0.043775 + 0.010271\exp(-0.55808y)$ |
| $a_{11}$ ..... | 0.8 |
| $a_{12}$ ..... | $0.34223 + 0.027134y - 0.0089229y^2 + 4.9996\times10^{-4}y^3$ |
| $a_{13}$ ..... | $-0.20480 + 0.013372y + 0.13087\exp(0.0044021(y-11.467)^2)$ |
| $a_{14}$ ..... | $a_1(x=-0.75)$ |
| | $\Delta(1232)$, eq. (17) |
| $b_{10}$ ..... | $18.712 + 18.030y + 5.8239y^2 + 0.62728y^3$ |
| $b_{11}$ ..... | $612.61 + 404.80y + 67.406y^2$ |
| $b_{12}$ ..... | $98.639 + 96.741y + 31.597y^2 + 3.4567y^3$ |
| $b_{13}$ ..... | $-208.38 - 183.65y - 53.283y^2 - 5.0470y^3$ |
| $b_{20}$ ..... | $0.21977 + 0.064073x$ |
| $b_{21}$ ..... | $3.3187\times10^3 + 3463.4y + 1.1982\times10^3y^2 + 136.71y^3$ |
| $b_{22}$ ..... | $91.410 + 91.613y + 30.621y^2 + 3.4296y^3$ |
| $b_{23}$ ..... | $-521.40 - 529.06y - 178.49y^2 - 19.975y^3$ |
| | res(1600), eq. (18) |
| $c_{10}$ ..... | $-1.5013 - 1.1281y - 0.19813y^2$ |
| $c_{11}$ ..... | $-33.179 - 22.496y - 3.3108y^2$ |
| $c_{12}$ ..... | $116.44 + 122.11y + 42.594y^2 + 4.9609y^3$ |
| $c_{13}$ ..... | $-545.77 - 574.80y - 201.25y^2 - 23.400y^3$ |
| $c_{20}$ ..... | $0.68849 + 0.36438y + 0.047958y^2$ |
| $c_{21}$ ..... | $-1.6871\times10^4 - 1.7412\times10^4y - 5.9648\times10^3y^2 - 679.27y^3$ |
| $c_{22}$ ..... | $-88.565 - 94.034y - 33.014y^2 - 3.8205y^3$ |
| $c_{23}$ ..... | $1.5141\times10^3 + 1.5757\times10^3y + 544.20y^2 + 62.446y^3$ |

Thus, $a_0$ is taken such that

$$a_0\int_0^\infty p_t\exp\left(-\frac{p_t}{a_1}\right)dp_t = \frac{\Delta\sigma}{\Delta\log(E)} \tag{10}$$

which gives

$$a_0 = \frac{1}{a_1^2}\frac{\Delta\sigma}{\Delta\log(E)} \tag{11}$$

and $\Delta\sigma/\Delta\log(E)$ is calculated using the parameterization of the inclusive cross section by Kamae et al. (2006).

Parameter $a_1$ is a function of both the gamma-ray energy, $E$, and the proton kinetic energy, $T_p$. It is first fitted as a function of $x = \log(E[\mathrm{GeV}])$ for each simulated proton kinetic energy. The formula describing $a_1$ is

$$a_1(x) = \begin{cases} a_{10}\exp\left(-a_{11}(x+a_{12})^2\right) & x \le -0.75, \\ a_{13}(x+0.75) + a_{14} & x > -0.75. \end{cases} \tag{12}$$

The parameters $a_{1i}$ $(i = 0,\ldots,4)$ are then given by functions of the proton kinetic energy, which are listed in Table 1.

For the baryon resonance components $\Delta\sigma/\Delta p_t^2$ will not follow the exponential form. Instead, $F(p_t, x)$ is fitted to a Gaussian form

$$F_{\Delta(1232)}(p_t, x) = b_0\exp\left(-\frac{(p_t-b_1)^2}{b_2}\right) \tag{13}$$

and

$$F_{\mathrm{res}(1600)}(p_t, x) = c_0\exp\left(-\frac{(p_t-c_1)^2}{c_2}\right). \tag{14}$$

With the requirement that the integral over $p_t$ should recover the inclusive cross section (eq. 9)

$$b_0 = 2(b_1\sqrt{\pi b_2}(\mathrm{erf}(b_1/\sqrt{b_2})+1) + \\ + b_2\exp(-b_1^2/b_2))^{-1}\frac{\Delta\sigma}{\Delta\log(E)} \tag{15}$$

and

$$c_0 = 2(c_1\sqrt{\pi c_2}(\mathrm{erf}(c_1/\sqrt{c_2})+1) + \\ + c_2\exp(-c_1^2/c_2))^{-1}\frac{\Delta\sigma}{\Delta\log(E)}. \tag{16}$$

Again, the parameters $b_i$ and $c_i$ $(i = 1, 2)$ are functions of both $E$ and $T_p$ and the same procedure is followed for them, with

$$b_i(x) = b_{i0}\exp\left(-b_{i1}\left(\frac{x-b_{i2}}{1.0+b_{i3}(x-b_{i2})}\right)^2\right) \tag{17}$$

and

$$c_i(x) = c_{i0}\exp\left(-c_{i1}\left(\frac{x-c_{i2}}{1.0+c_{i3}(x-c_{i2})}\right)^2\right), \tag{18}$$

for $x < 0.5$ and $b_i(x) = 0$ for $x \ge x_b$ and $c_i(x) = 0$ for $x \ge x_c$, with

$$x_b = 0.81(y+3.32) - 0.5 \tag{19}$$

$$x_c = 0.82(y+3.17) - 0.25, \tag{20}$$

where $y = \log(T_p[\mathrm{TeV}])$. These limits of $b_i$ and $c_i$ were introduced to control artifacts near the kinematical limits. The parameters $b_{ij}$ and $c_{ij}$ $(j = 0,\ldots,4)$ are listed in Table 1 as functions of the proton kinetic energy.

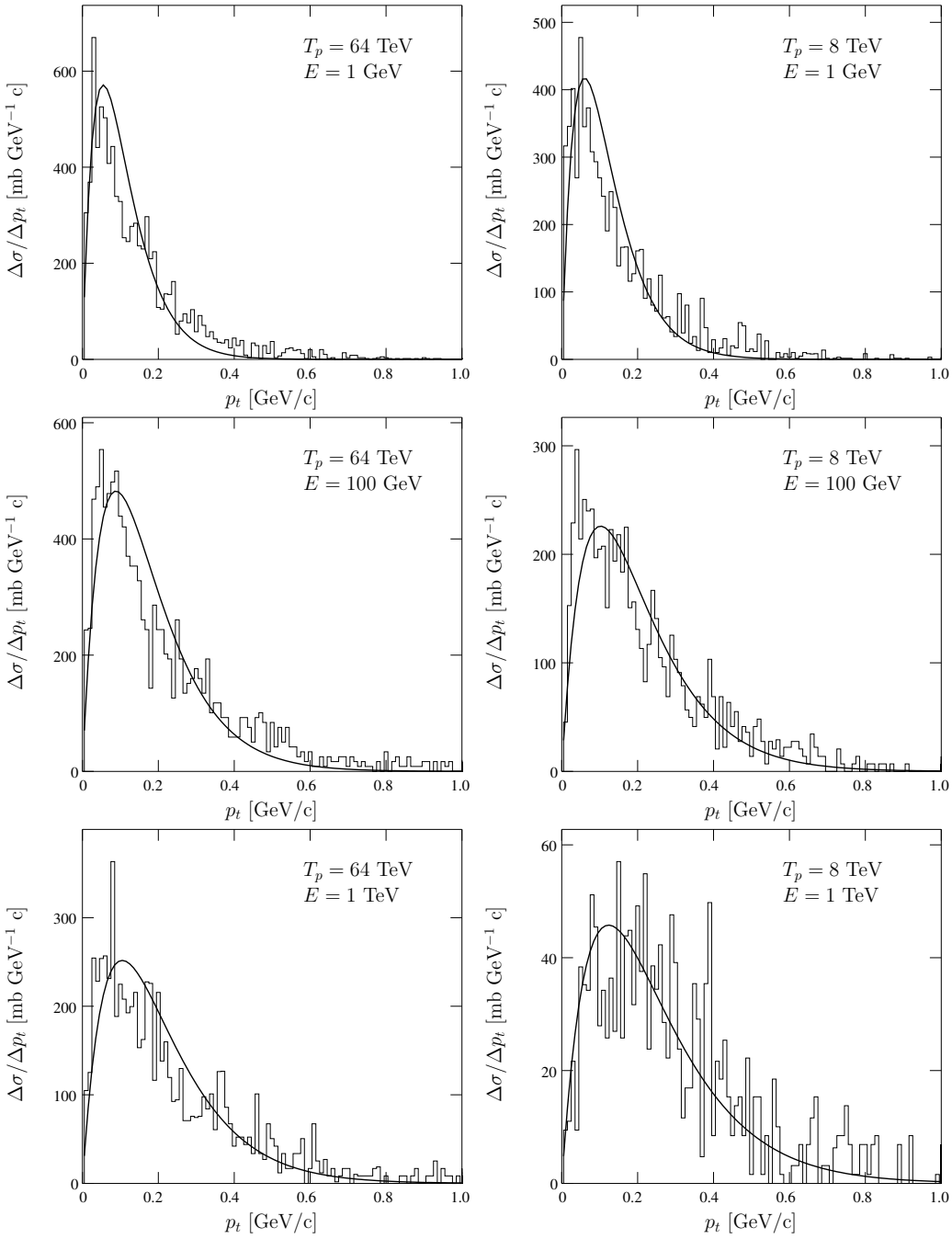


FIG. 4.— Gamma-ray differential cross section $\Delta\sigma/\Delta p_t$ for the non-resonance contribution calculated using the parameterization (thick solid line) and superimposed with the Monte Carlo simulated cross section (thin histogram). Panels on the left-hand side are for proton kinetic energy $T_p = 64$ TeV and panels on the right-hand side are for $T_p = 8$ TeV. Rows are for gamma-ray energy $E = 1$ GeV (top), 100 GeV (middle), and 1 TeV (bottom).

Figure 4 shows the gamma-ray differential cross section $\Delta\sigma/\Delta p_t$ for the non-resonance contribution calculated using the above described parameterization for proton kinetic energies $T_p = 64$ TeV and 8 TeV and gamma-ray energies $E = 1$ GeV, 100 GeV and 1 TeV. The plots show how the average transverse momentum, $\langle p_t \rangle$, increases with increasing gamma-ray energy. Figure 5 shows $\Delta\sigma/\Delta p_t$ for the two resonance contributions, $\Delta(1232)$ and res(1600), calculated at proton kinetic energy $T_p = 0.82$ GeV and gamma-ray energy $E = 0.3$ GeV. Superimposed in both figures are the differential cross sections from the Monte Carlo simulations. The agreement is in general good except near the higher and lower kinematical limits where low statistics in the Monte Carlo simulations limits accuracy of the fit.

## 5. APPLICATION OF FORMULAE

The parameterized model of stable secondary particle spectra by Kamae et al. (2006) was used to predict differences in the diffuse gamma-ray spectrum from the Galactic ridge compared with the scaling models implemented in Galprop. The present model finds its application in scenarios where the gamma-ray spectrum is expected to be angular dependent, such as AGN jets and GRBs, but

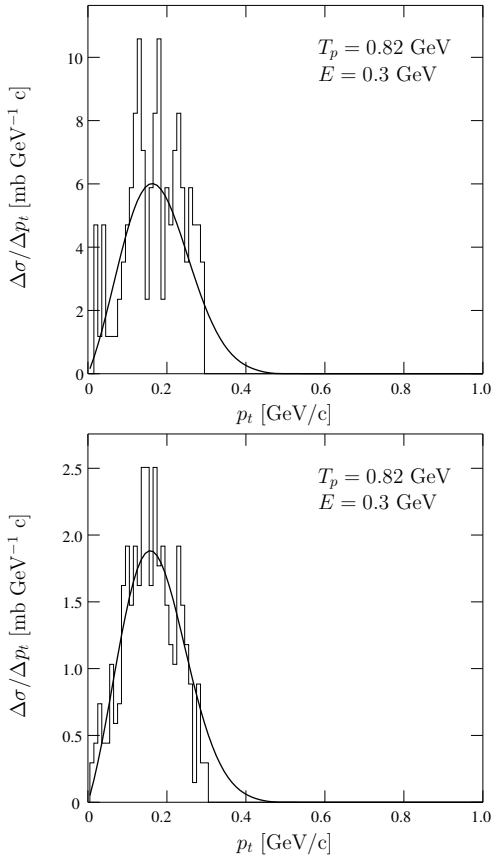


FIG. 5.— Gamma-ray differential cross section $\Delta\sigma/\Delta p_t$ for the two resonance contributions, $\Delta(1232)$ and res(1600), calculated using the parameterization (thick solid line) and superimposed with the Monte Carlo simulated cross section (thin histogram) for proton kinetic energy $T_p = 0.82$ GeV and $E = 0.3$ GeV. The top panel is for for the $\Delta(1232)$ resonance and the bottom panel is for the res(1600) resonance.

SNRs may also fall into this category. The highest-energy CR escape the forward shock almost unidirectionally giving rise to beaming in SNRs.

To demonstrate the use of the parameterized formulae for gamma-ray $p_t$ distributions, the gamma-ray spectrum has been calculated for two different cases; the first is a pencil beam of protons following a power law of index 2.0 and the other is a fanned proton jet with a Gaussian angular profile impinging on the surrounding matter.

### 5.1. *Pencil Beam of Protons*

Consider a beam of protons along the z-axis with no spatial extension in the x-y plane, i.e. a pencil beam. The energy distribution of protons is assumed to be a power law, $dN/dE = T_p^{-s}$, with index $s = 2.0$ and extending up to $T_p = 512$ TeV. The gamma-ray spectrum, $E^2dF/dE$, is calculated for three different observation angles $\theta = 0°$ (head on), $0\overset{\circ}{.}5$, and $2°$ relative to the beam axis. The spectra, which are shown in Figure 6, are integrated over the annular portion $(\theta, \theta + d\theta)$ of width $d\theta = 2'$. The absolute normalization is relative to the density and distribution of target protons. For comparison the spectrum integrated over the entire phase space is also plotted in the figure. As can be seen in the figure, the gamma-ray emission is peaked in the very forward direction. When the viewing angle is increased, the peak

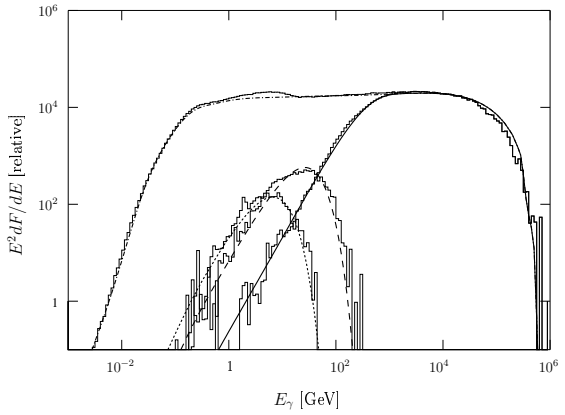


FIG. 6.— Gamma-ray spectra from a pencil beam of protons observed from three different angles, $\theta = 0°$ (solid), $0\overset{\circ}{.}5$ (dashed), and $2°$ (dotted) calculated using the parametric model. The spectra are integrated over the annular portion $(\theta, \theta + d\theta)$ of width $d\theta = 2'$. Included is also the spectrum integrated over the entire phase space (dash-dotted). Histograms are the corresponding Monte Carlo spectra. The protons in the beam are assumed to follow a power law in kinetic energy, $T_p$, with index 2.0 and extending up to $T_p = 512$ TeV. Fluctuations in the histograms are due to low event statistics

of the spectrum is shifted to lower gamma-ray energies and the the flux decreases rapidly. Fluctuations in the histograms are due to low event statistics.

### 5.2. *Fanned Proton Jet*

The second example is a fanned proton jet which features a Gaussian intensity profile centered on the jet axis. With a FWHM of $3°$ the opening angle of the jet is about $10°$. The gamma-ray spectrum of the jet is integrated over the intensity profile, which is sampled in $0\overset{\circ}{.}1 \times 0\overset{\circ}{.}1$ bins, where each bin is represented by the average of ten randomly sampled pencil beams pointing within the bin. Protons in the jet are again assumed to follow a power-law distribution with index $s = 2.0$ and extending up to $T_p = 512$ TeV. The gamma-ray spectra, calculated per solid angle, observed from four different angles, $\theta = 0°$ (head on), $5°$, $10°$, and $20°$ are shown in Figure 7. As with the pencil beam spectra, the absolute normalization is relative to the density and distribution of target protons.

When the viewing angle is smaller than the opening angle of the jet the gamma-ray spectrum features a tail extending up to the highest possible gamma-ray energy, about $10^6$ GeV, as can be seen in Figure 7. The tail is suppressed for larger viewing angles because of the Gaussian intensity profile. At $\theta = 5°$ the tail is about four orders of magnitude lower in flux.

## 6. CONCLUSIONS AND FUTURE PROSPECTS

The angular distribution of gamma-rays produced by proton-proton interactions have been presented in parameterized formulae. The formulae were derived from Monte Carlo simulations of the up-to-date proton-proton interaction model by Kamae et al. (2006) and they facilitate computation of gamma-ray spectra in cases of anisotropic proton distributions. The formulae incorporate all important known features of the proton-proton interaction up to about $T_p = 500$ TeV.

As an example of the application of the formulae, gamma-ray spectra was calculated for different viewing

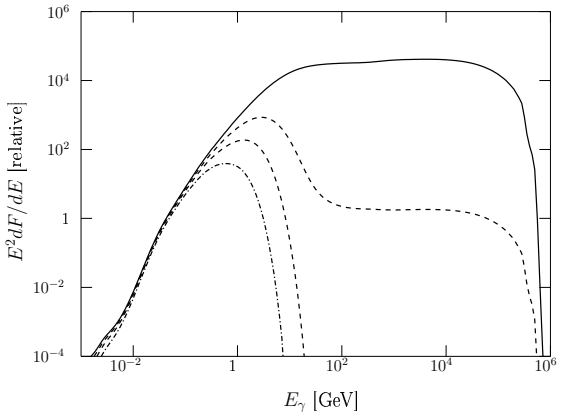


FIG. 7.— Gamma-ray spectra, calculated per solid angle, from a proton jet, with a Gaussian intensity profile (FWHM 3°) centered on the jet axis, observed from four different angles, $\theta = 0°$ (solid) 5° (dashed), 10° (dotted), and 20° (dot-dashed). The protons in the jet are assumed to follow a power-law distribution with index $s = 2.0$ and extending up to $T_p = 512$ TeV.

angles from a pencil beam of protons as well as a proton jet with an Gaussian intensity profile. The pencil beam example shows very clearly that the gamma-ray spectrum changes significantly as the observer is moved off the beam. The gamma-ray flux decreases drastically and the spectrum gets cut off at lower energy.

The jet with a Gaussian intensity profile provides a more realistic example. The flux does not decrease as drastic, but the spectrum changes significantly. For on-axis observers the spectrum features a prominent tail which is suppressed as the observer is moved off axis. The peak of the spectrum is shifted to lower energies as the observer is moved.

Particle acceleration models predict some degree of anisotropy for the highest-energy particles escaping from the acceleration site. The parameterized model presented here can be used to calculated the anisotropy in gamma-ray emission for any given anisotropy in the proton distribution.

The implementation of formulae and parameters given in this paper in a C language library will be made available as supplementary online material. The functions implemented in this library can be used to calculate both the parameters in Table 1 for any given $T_p$ and the differential cross section in equation 5 using those parameters for any given set of $E$ and $p_t$.

The authors would like to acknowledge valuable discussions with and comments received from T. Abe, K. Andersson, P. Carlson, J. Chiang, J. Cohen-Tanugi, S. Digel, E. do Couto e Silva, T. Koi, G. Madejski, T. Mizuno, I. Moskalenko, M. Müller, P. Nolan, A. Reimer, O. Reimer, T. Sjöstrand, H. Tajima and L. Wai.

N. Karlsson is grateful for the hospitality extended to him by SLAC and KIPAC and the encouragement given by R. Blandford, S. Kahn and P. Drell.

This work was supported in part by the U.S. Department of Energy under Grant DE-AC02-76SF00515.

## REFERENCES

Abe, F. et al. 1988, Phys. Rev. Lett., 61, 1819
Aharonian, F. A. 2004, Very High Energy Cosmic Gamma Radiation: A Crucial Window on the Extreme Universe (World Scientific Publishing)
Aharonian, F. A. et al. 2003, A&A, 403, L1
—. 2004a, Nature, 432, 75
—. 2004b, A&A, 425, L13
—. 2005, Science, 307, 1938
Alner, G. J. et al. 1987, Physics Reports, 154, 247
Alper, B. et al. 1975, Nucl. Phys., B100, 237
Banner, M. et al. 1982, Phys. Lett., 115B, 59
—. 1983, Phys. Lett., 122B, 322
Beilicke, M. et al. 2005, in Proceedings of the 29th International Cosmic Ray Conference, ed. B. S. Acharya et al., Pune, India
Berezhko, E. G. & Volk, H. J. 2000, ApJ, 540, 923
Bicknell, G. V. & Begelman, M. C. 1996, ApJ, 467, 597
Blattnig, S. R. et al. 2000, Phys. Rev. D, 62, 094030
Böttcher, M. & Reimer, A. 2004, ApJ, 609, 576
Crawford, J. F. et al. 1980, Phys. Rev., C22, 1184
Dermer, C. D. 1986a, A&A, 157, 223
—. 1986b, ApJ, 307, 47
Enomoto, R. et al. 2002, Nature, 416, 823
Hagiwara, K. et al. 2002, Phys. Rev., D66, 010001
Halzen, F. 2005, in AIP Conference Proceedings, Vol. 745, 2nd International Symposium on High Energy Gamma-Ray Astronomy, ed. F. A. Aharonian, H. J. Völk, & D. Horns (New York: AIP), 3–13
Hartman, R. C. et al. 1999, ApJS, 123, 79
Hayakawa, S. 1969, Cosmic Ray Physics (John Wiley & Sons)
Hunter, S. D. et al. 1997, ApJ, 481, 205
Iyudin, A. F. et al. 2005, A&A, 429, 225
Kamae, T., Abe, T., & Koi, T. 2005, ApJ, 620, 244
Kamae, T. et al. 2006, ApJ, 647, 692, (erratum 662, 779)
Katagiri, H. et al. 2005, ApJ, 619, L163
Koers, H. B. J., Pe'er, A., & Wijers, R. A. M. J. 2006, preprint (hep-ph/0611219)
Koyama, K. et al. 1997, PASJ, 49, L7
Mori, M. 1997, ApJ, 478, 225
Moskalenko, I. V. et al. 2007, in Proceedings of the 30th International Cosmic Ray Conference, Merida, Mexico
Mårtensson, J. et al. 2000, Phys. Rev., C62, 014610
Mücke, A. & Protheroe, R. J. 2001, Astroparticle Physics, 15, 121
Mücke, A. et al. 2003, Astroparticle Physics, 18, 593
Murthy, P. V. R. & Wolfendale, A. W. 1986, Gamma-Ray Astronomy (Cambridge University Press)
Ong, R. A. 1998, Physics Reports, 305, 93
Reimer, A., Protheroe, R. J., & Donea, A.-C. 2004, A&A, 419, 89
Rossi, A. M. et al. 1975, Nuclear Physics, B84, 269
Schlickeiser, R. 2002, Cosmic Ray Astrophysics (Springer)
Schönfelder, V. 2001, The Universe in Gamma Rays (Springer)
Schroedter, M. et al. 2005, ApJ, 634, 947
Sjöstrand, T. & Skands, P. Z. 2004, preprint (hep-ph/0402078)
Sjöstrand, T. et al. 2001, Comput. Phys. Commun., 135, 238
Slane, P. et al. 1999, ApJ, 525, 357
Stawarz, L. et al. 2006, MNRAS, 370, 981
Stecker, F. W. 1970, Ap&SS, 377
—. 1973, ApJ, 185, 499
—. 1989, Cosmic Gamma Rays, Neutrinos and Related Astrophysics, ed. M. M. Shapiro & J. P. Wefel (Kluwer Academic Publishers), 85–120
Stephens, S. A. & Badhwar, G. G. 1981, Ap&SS, 76, 213
Strong, A. W., Moskalenko, I. V., & Ptuskin, V. S. 2007, Annu. Rev. Nucl. Part. Sci., 57, 285
Strong, A. W., Moskalenko, I. V., & Reimer, O. 2000, ApJ, 537, 763, (erratum 541, 1109)
—. 2004, ApJ, 613, 962
Strong, A. W. et al. 1978, MNRAS, 182, 751
—. 1982, A&A, 115, 404
Tsunemi, H. et al. 2000, PASJ, 52, 887
Uchiyama, Y., Aharonian, F. A., & Takahashi, T. 2003, A&A, 400, 567
Weekes, T. C. 2003, in Proceedings of the 28th International Cosmic Ray Conference, Tsukuba, Japan